O18+Se76 elastic and inelastic scattering at 275 MeV

09 August 2024

$^{18}O + ^{76}Se$ elastic and inelastic scattering at 275 MeV

L. La Fauci,[1,2,*] A. Spatafora,[1,2] F. Cappuzzello,[1,2] C. Agodi,[1] D. Carbone,[1] M. Cavallaro,[1] J. Lubian,[3] L. Acosta,[4] P. Amador-Valenzuela,[5] T. Borello-Lewin,[6] G. A. Brischetto,[1,2] S. Calabrese,[1,2] D. Calvo,[7] V. Capirossi,[7,8] E. R. Chàvez Lomelí,[4] I. Ciraldo,[1,2] M. Cutuli,[1,2] F. Delaunay,[7,8,9] H. Djapo,[10] C. Eke,[11] P. Finocchiaro,[1] S. Firat,[12] M. Fisichella,[7] A. Foti,[13] M. A. Guazzelli,[14] A. Hacisalihoglu,[1,15] F. Iazzi,[7,8] R. Linares,[3] J. Ma,[16] N. H. Medina,[6] M. Moralles,[17] J. R. B. Oliveira,[6] A. Pakou,[18] L. Pandola,[1] H. Petrascu,[19] F. Pinna,[7,8] P. C. Ries,[20] G. Russo,[2,13] O. Sgouros,[1] S. O. Solakci,[12] V. Soukeras,[1] G. Souliotis,[21] D. Torresi,[1] S. Tudisco,[1] J. Wang,[16,22] Y. Yang,[16] A. Yildirin,[12] and V. A. B. Zagatto[3]
(NUMEN collaboration)

[1]*Istituto Nazionale di Fisica Nucleare, Laboratori Nazionali del Sud, I-95123 Catania, Italy*
[2]*Dipartimento di Fisica e Astronomia "Ettore Majorana", Università di Catania, I-95123 Catania, Italy*
[3]*Instituto de Fisica, Universidade Federal Fluminense, 24210-340 Niterói, Rio de Janeiro, Brazil*
[4]*Instituto de Fisica, Universidad Nacional Autónoma de México, 04510 México City, Mexico*
[5]*Instituto Nacional de Investigaciones Nucleares - Ocoyoacac 52750, Mexico*
[6]*Instituto de Fisica, Universidade de São Paulo, 05508-060 São Paulo, Brazil*
[7]*Istituto Nazionale di Fisica Nucleare, Sezione di Torino, I-10124 Torino, Italy*
[8]*Dipartimento Scienza Applicata e Tecnologia, Politecnico di Torino, I-10129 Torino, Italy*
[9]*Laboratoire de Physique Corpusculaire de Caen, Normandie Université, ENSICAEN, UNICAEN, CNRS/IN2P3, F-14000 Caen, France*
[10]*Ankara University, Institute of Accelerator Technologies, 06100 Ankara, Turkey*
[11]*Department of Mathematics and Science Education, Akdeniz University, 07058 Antalya, Turkey*
[12]*Department of Physics, Akdeniz University - 07070 Antalya, Turkey*
[13]*Istituto Nazionale di Fisica Nucleare, Sezione di Catania, I-95123 Catania, Italy*
[14]*Centro Universitàrio FEI - São Bernardo do Campo 09850-305, Brazil*
[15]*Institute of Natural Science, Karadeniz Teknik Universitesi, 61080 Trabzon, Turkey*
[16]*Institute of Modern Physics, Chinese Academy of Sciences - 730000 Lanzhou, China*
[17]*Instituto de Pesquisas Energeticas e Nucleares IPEN/CNEN, 05508-000 Sao Paulo, Brazil*
[18]*Department of Physics, University of Ioannina and Hellenic Institute of Nuclear Physics, 451 10 Ioannina, Greece*
[19]*Institutul National de Cercetare-Dezvoltare pentru Fizica si Inginerie Nucleara Horia Hulubei, 077125 Bucarest, Romania*
[20]*Institut fur Kernphysik, Technische Universität Darmstadt, 64289 Darmstadt, Germany*
[21]*Department of Chemistry, University of Athens and Hellenic Institute of Nuclear Physics, 157 72 Athens, Greece*
[22]*Huzhou University, Huzhou, 313000 Zhejiang Province, China*

(Received 19 December 2020; revised 6 October 2021; accepted 10 November 2021; published 29 November 2021)

Background: An accurate description of the initial and final state interactions in the $^{18}O + ^{76}Se$ collision is demanded by the NUMEN project. The study of single and double charge exchange nuclear reactions is the main purpose for NUMEN, since these can be used as tools to provide experimentally driven information about nuclear matrix elements of interest in the context of neutrinoless double-β decay. To date, the details of the optical potentials and nuclear response to isospin operators for many of the projectile-target systems proposed for the NUMEN double charge exchange studies are poorly known. The $^{18}O + ^{76}Se$ case, here under study, is particularly relevant due to its connection with the ^{76}Ge neutrinoless double-β decay.
Purpose: In this work the authors want to characterize the initial-state interaction for the $^{18}O + ^{76}Se$ reactions at 275 MeV incident energy determining the optical potential and evaluating the effect of couplings with the inelastic scattering on the elastic channel.
Methods: The angular distributions of differential cross section were measured in the angular region between 4° and 22° in the center-of-mass reference frame. The cross sections were compared with theoretical calculations, that adopt different optical potentials. Coupling effects on the elastic channel were determined into the coupled channels formalism.
Results: The excitation energy spectrum of the colliding nuclei and the cross section angular distributions were measured with satisfactory energy resolution. The elastic scattering cross section is not well reproduced in the full angular range explored when the optical model approach is adopted. A good agreement is found using

*lauralafauci1985@hotmail.it

coupled channel calculations. The initial state interaction for the $^{18}O + ^{76}Se$ nuclear reactions at 275 MeV is determined.

Conclusions: Coupled channels effects are crucial to obtain a good description of the measured elastic and inelastic channels cross sections, even at large transferred momenta where the optical model approach fails in reproducing the experimental data. The role of channel coupling could be relevant also in the analysis of other open reaction channels in the same collision and should be accounted for in double charge exchange analyses as well.

DOI: 10.1103/PhysRevC.104.054610

I. INTRODUCTION

The study of single (SCE) and double charge exchange (DCE) nuclear reactions induced by heavy ions is of particular interest since connected with double-β decay [1,2]. The NUMEN (nuclear matrix elements for neutrinoless double-β decay) and NURE (nuclear reactions for neutrinoless double-β decay) [3,4] projects aim to study SCE and DCE reactions in order to obtain information on the nuclear matrix elements (NME) entering in the expression of the half-lives of neutrinoless double-β decay ($0\nu\beta\beta$).

One of the main goals of the NUMEN and NURE projects is to develop a complete and consistent theoretical approach to extract accurate estimations of the NME for $0\nu\beta\beta$ from the DCE reactions. In particular, a clear view over the initial and final state interactions is necessary for an accurate description of the SCE and DCE reaction mechanisms. To date, the existing information about the optical potential (OP) for the systems of interest is indeed limited and not deeply tested.

Elastic scattering is the main tool for probing the initial state interaction (ISI) [5–7]. It is the most probable process, so describing it is a necessary first step to obtain a realistic representation of the nucleus-nucleus interaction. The comparison of the elastic scattering cross sections with the optical model (OM) calculations gives crucial information on the nucleus-nucleus OP, which is the most important part of the interaction between the colliding nuclei prior to the nuclear reaction. A practical way to find a reasonable ISI is to describe the elastic scattering using an OP with a Woods-Saxon shape, adjusting its parameters to describe the measured elastic cross sections [6]. However, such an effective approach hides the physical insight and has been less adopted in analyses of direct nuclear reactions and would not be predictive at all for other systems where the elastic channel is not experimentally measurable, e.g., for the core-core potentials involved in the multinucleon transfer reactions [8]. To date, the best models to determine the OP in heavy-ion collisions are obtained by folding the frozen densities of the colliding nuclei with a realistic nucleon-nucleon interaction. In such cases, the frozen densities approximation is justified by the strong absorption in heavy-ion collisions that bounds the reaction source near the surfaces of the colliding nuclei making the reaction mechanism insensitive to the internal regions [6,9].

Detailed analyses of $^{16}O + ^{16}O$ elastic scattering at different energies reported in Refs. [10,11] demonstrated that the peculiar diffractive patterns, observed in the experimental cross section angular distributions, are due to couplings with the low-lying inelastic excited states. More recent works [12–17] have emphasized the role of the nuclear deformation and coupling to low-lying inelastic transitions for a satisfactory description of a large body of elastic scattering data involving $^{12,13}C$ and ^{16}O induced collisions up to high transferred momentum (several fm^{-1}). The relevance of the couplings to inelastic channels was also investigated by NUMEN for the $^{20}Ne + ^{76}Ge$ reaction at 15.3A MeV incident energy [18]. It was seen that contributions due to the couplings with the inelastic scattering channels are important when large transferred momenta are involved, indicating that the couplings effects cannot be considered *a priori* negligible.

The work here presented is focused on the experimental and theoretical analysis of the elastic and inelastic channels of the $^{18}O + ^{76}Se$ collisions at 15.3A MeV incident energy, performed at INFN Laboratori Nazionali del Sud (LNS) in Catania, within the NUMEN project. The study of this system is relevant for the NUMEN purposes for its relation with the ^{76}Ge $0\nu\beta\beta$ decay NME. ^{76}Se is indeed the daughter nucleus in the $0\nu\beta\beta$ decay of ^{76}Ge and the residual/target nucleus in the $^{76}Ge(^{20}Ne, ^{20}O)^{76}Se$ and $^{76}Se(^{18}O, ^{18}Ne)^{76}Ge$ DCE reactions under study within the NUMEN project at 15.3A MeV.

The theoretical description of both reaction mechanisms requires an accurate determination of the ISI, which represents a key aspect for these studies. To our knowledge, no study of the $^{18}O + ^{76}Se$ elastic scattering is available in the literature. In many studies the ^{18}O was used as a nuclear probe [19–23] and in many others the ^{76}Se was used as target [24–27]. In all of them the experimental conditions were very different from those in which the experiment here described was performed.

In some works [28,29], it was demonstrated that for the description of the ^{18}O reaction mechanism an enlargement of the diffuseness is mandatory. As was seen in similar works [12,18], this property suggests that contributions to the ISI due to the couplings with inelastic and other direct reaction channels might be significant at the explored transferred momentum.

To determine the effect of the inelastic channel on the ISI, a coupling scheme that includes the first excited states of the colliding nuclei is considered. In particular, the role of the first low-lying excitation of the projectile and the target is investigated. This study compares elastic scattering data and calculations performed in the OM and in the coupled channels (CC) formalism. For the inelastic channels, results obtained using the distorted wave Born approximation (DWBA) and CC approaches were compared.

In Sec. II, details of the experimental setup and experimental results are presented. The theoretical framework and

the comparison between different tested OPs, are discussed in Sec. III. The main theoretical results, based on the comparison of the experimental data and calculations performed with the OM, DWBA, and CC approaches are discussed in Sec. IV. Finally, conclusions are reported in Sec. V.

II. EXPERIMENT AND DATA REDUCTION

A ^{18}O beam was accelerated by the K800 superconducting cyclotron [30] at the Laboratori Nazionali del Sud of Istituto Nazionale di Fisica Nucleare and the fully stripped ions were transported to the object point of the MAGNEX large acceptance magnetic spectrometer [31]. The target was a layer of $280 \pm 15\ \mu$g/cm^2 ^{76}Se (purity $99.8 \pm 0.1\%$), evaporated onto a $80 \pm 4\ \mu$g/cm^2 natural carbon backing. A copper Faraday cup (FC) (0.8 cm diameter and 3 cm depth) was used to stop the beam and measure the beam charge. It was located 15 cm downstream of the target. An electron suppressor polarized at -200 V and a low noise charge integrator allowed a charge collection accuracy better than 10%.

The ^{18}O ejectiles, scattered by the ^{76}Se and C target atoms present in the target, were analyzed in momentum by the MAGNEX spectrometer. The optical axis of MAGNEX was set at $\theta_{\rm opt} = 8^\circ$, 14°, and 18° with respect to the beam direction in four different data sets. The 50 msr angular acceptance of MAGNEX was set by means of horizontal and vertical slits at the entrance of the spectrometer. The angular overlap between adjoining measurements was about 6° in the laboratory reference frame. The overall measured angular range in the center-of-mass reference frame was $4^\circ \lesssim \theta_{\rm c.m.} \lesssim 22^\circ$. For each angular setting, the beam flux was adjusted in order to ensure a maximum event rate of about 100 counts per second in the focal plane detector (FPD) [32,33] of MAGNEX.

Under this rate limit, a good resolution in the tracking of ejectiles as well as in the particle identification was achieved in all the measured runs and over the whole volume covered by the FPD. At $\theta_{\rm opt} = 8^\circ$, where the elastic cross section at forward angles is very high, the beam current was optimized to about 100 epA. With this current the used FC and the charge integrator were not able to ensure an acceptable signal to noise ratio. In order to renormalize the cross sections measured at very forward angles ($6^\circ \lesssim \theta_{\rm lab} \lesssim 14^\circ$), further data were collected at the same central angle, but excluding the forward angle region by the MAGNEX entrance slits. In this way it was possible to increase the beam current up to measurable values (about 4 enA).

The data reduction procedure consists of many phases: the calibration of the vertical and horizontal positions and angles measured by the MAGNEX FPD [34]; the identification of the $^{18}O^{8+}$ ejectiles of interest [35–38]; the determination of the transport matrix and its inversion to perform the trajectory reconstruction procedure [39]. The latter is based on the fully differential algebraic method implemented in the MAGNEX spectrometer. The measured ion positions and angles are used as input of the high order ray-reconstruction algorithms that guarantees an effective compensation of the aberrations generated by the large aperture magnetic elements of the spectrometer [40]. As a result, the phase space parameters are reconstructed back to the target point for the selected ^{18}O ejectiles. These are then transformed, by the application of relativistic two-body kinematics relations, in the scattering angle and kinetic energy of the detected ejectiles. The overall detection efficiency was determined following the prescription of Ref. [33] that is a crucial information to extract the absolute cross section from the collected event yields.

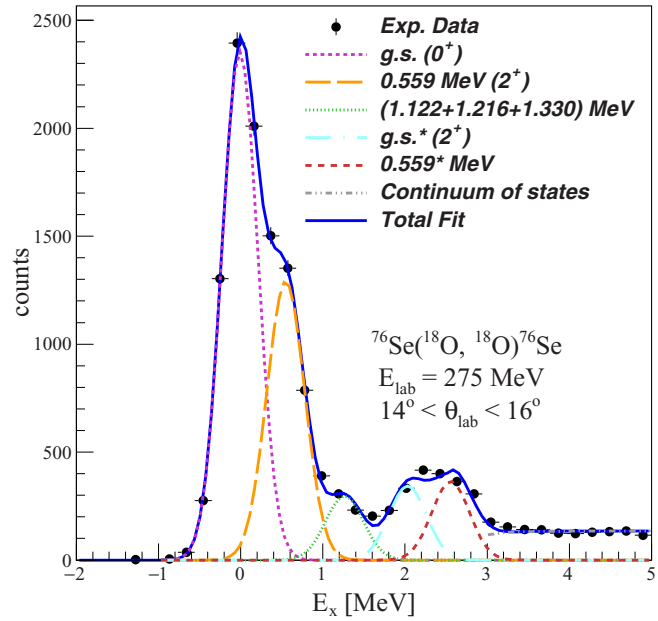

FIG. 1. Excitation energy spectrum for ^{18}O + ^{76}Se elastic scattering at 275 MeV, fitted by a multiple-fit procedure. In the legend the meaning of the different coloured lines is described. Asterisks identify states in which the ^{18}O ejectile is in its first 2^+ state at E_x = 1.982 MeV.

The achieved angular and energy resolutions are $\delta\theta_{\rm lab} \approx 0.7^\circ$ and $\delta E \approx 0.5$ MeV full width at half-maximum. Figure 1 shows an example of excitation energy (E_x) spectrum for the ^{18}O + ^{76}Se of the elastic and inelastic scattering obtained in the angular region $14^\circ < \theta_{\rm lab} < 16^\circ$. A multiple-fit analysis of the spectra was performed at all the angles following the same method also described in Ref. [18]. Here, the width of each Gaussian peak was fixed according to the energy resolution and the Doppler broadening due to the in-flight γ decay of the ejectile excited states. The first observed peak is described as the superposition of the dominant ground state (g.s.) and the first low-lying 2^+ state of ^{76}Se at $E_x = 0.559$ MeV. The structure at $E_x \simeq 1.2$ MeV corresponds to the 0^+(1.122 MeV), 2^+(1.216 MeV), 4^+(1.330 MeV) [41] triplet states of ^{76}Se. The first 2^+ state of ^{18}O at $E_x = 1.982$ MeV and the $2^+ \oplus 2^+$ transition corresponding to the excitation of the first 2^+ low-lying states of both projectile and target nuclei at $E_x \simeq 2.541$ MeV are visible in Fig. 1 and included in the multiple-fit procedure. The contribution due to the many unresolved states of projectile and target populated above 3 MeV is considered as a unique continuum.

Experimental cross section angular distributions for the elastic channel are presented in Fig. 2. The error bars include

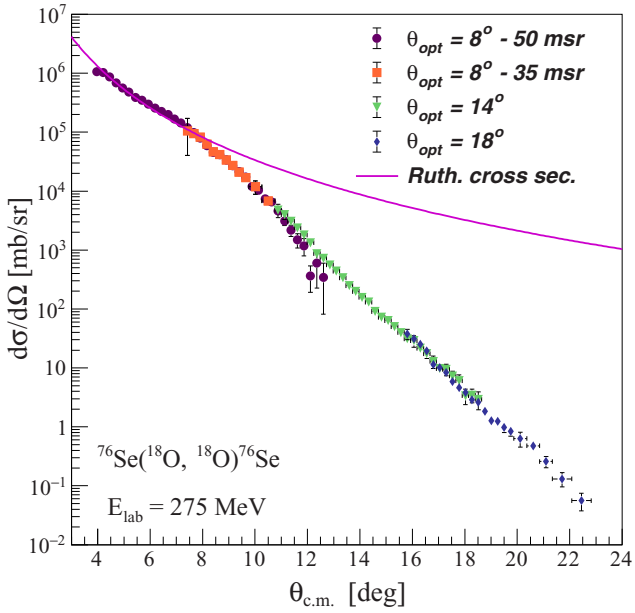

FIG. 2. Experimental cross section angular distributions for the elastic channel of the $^{18}O + ^{76}Se$ collision at 275*A* MeV. Different colors show the results obtained with the different angles of the optical axis of the MAGNEX spectrometer.

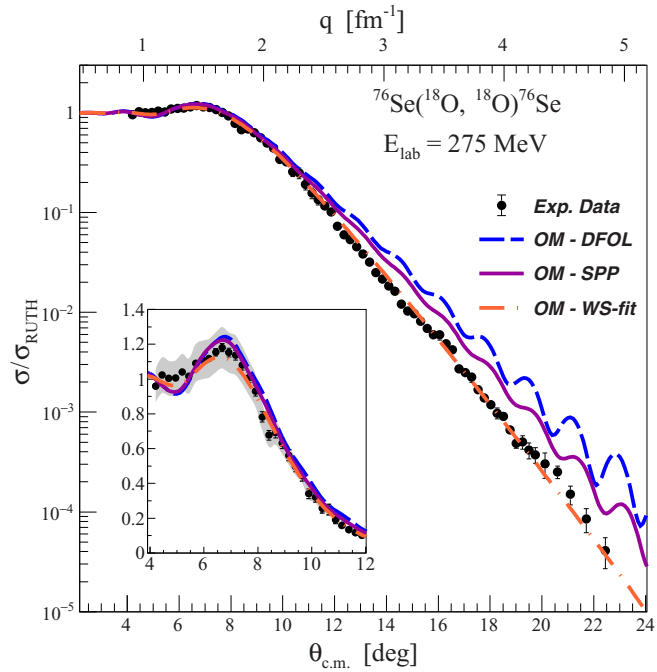

FIG. 3. Experimental cross section angular distribution in terms of its ratio with the Rutherford cross section for the $^{18}O + ^{76}Se$ elastic scattering at 275 MeV. The blue dashed line represents the DFOL calculations and the magenta continuous line the SPP ones. The theoretical curves are folded with the experimental angular resolution. The orange dot-dashed line represents the WS-fit calculation (see text). Inset: zoomed view of the Coulomb nuclear interference region. The experimental data are shown together with a grey band corresponding to the 10% uncertainty due to the charge collection and target thickness (see text).

the statistical error and the uncertainties coming from the fitting procedure and from the differential solid angle evaluation. The systematic error, due to the uncertainty in the charge collection and in the measurement of the number of scattering centres in the target, is not explicitly included in the error bars because common to all the points and has been estimated in experiments performed in similar conditions to be less than 10%. No scale factor was applied to the cross sections measured for all the elastic and inelastic transitions. The good agreement at very forward angles with the Rutherford cross section and the one between the cross sections obtained in independent measurements, performed in different settings of the optical angle, is a clear proof that the systematic error components are very small.

The elastic cross section expressed in terms of the ratio to Rutherford one is reported in Fig. 3. The Coulomb field dominates the scattering up to the grazing angle, located at $\theta_{\rm graz} \simeq 10.2^\circ$ in the c.m. reference frame. In the region beyond $\theta_{\rm graz}$, data are more sensitive to the nuclear component of the nucleus-nucleus potential, showing the typical fall-off associated with near-side scattering amplitudes. Differential cross section angular distributions have been extracted also for the transition to the first 2^+ states of projectile and target and for the simultaneous excitation of both of them and are shown in Fig. 4.

III. THEORETICAL ANALYSIS

In order to determine the ISI for all the nuclear reactions induced by the $^{18}O + ^{76}Se$ collision at 15.3*A* MeV, the search of a proper OP, the choice of the coupling scheme and the evaluation of coupling effects are mandatory. The calculations were performed using the FRESCO code [42] in OM, DWBA, and CC for different OPs and were compared with elastic and inelastic scattering data to investigate the role of those choices.

A. Study of the optical potential

The theoretical description of the elastic and inelastic scattering was performed using an OP:

$$U_{\rm opt} = V(r) + iW(r), \tag{1}$$

where the absorptive-imaginary part accounts for all the effects on the elastic cross section due to the nonexplicit inclusion of states and reaction channels in the assumed reduced coupling scheme. A first theoretical analysis was performed using the simplest approach in which only the elastic channel is included. This allows to compare the effects of the choice of the OP.

Two double folding optical potentials, DFOL [43] and São Paulo potential (SPP) [13,44], were compared. In the double-folding approach the heavy-ion nuclear potential depends on the nuclear densities of the colliding nuclei, as the real part of the potential is obtained by the folding of the nucleon-nucleon interaction $V_{NN}(\mathbf{r_1}, \mathbf{r_2}, E)$ with the ground state densities of

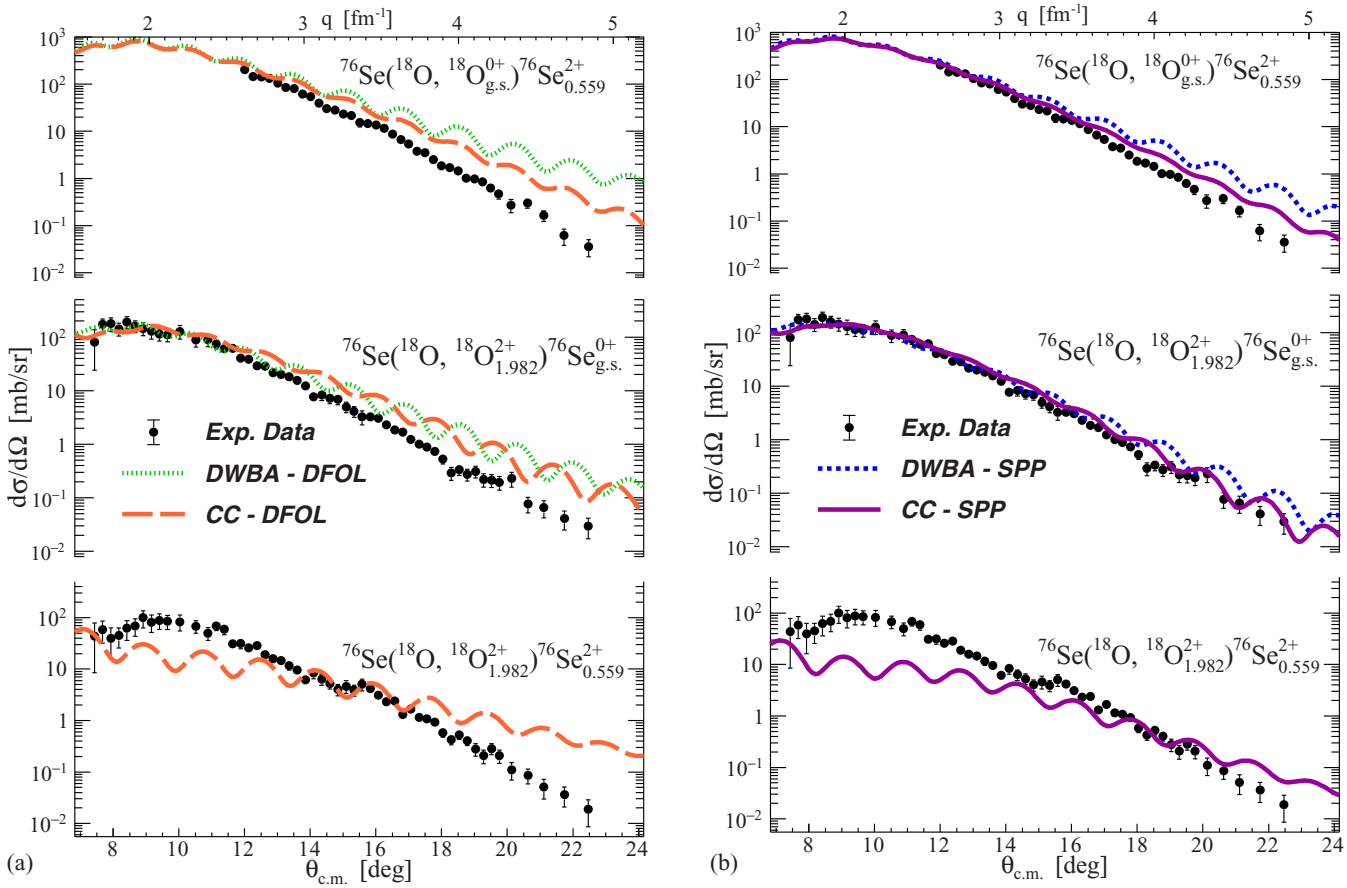

FIG. 4. Comparison between the experimental cross section angular distributions of ^{18}O + ^{76}Se and calculations in DWBA and CC approaches with DFOL (a) and SPP (b) potentials. The theoretical curves are folded with the experimental angular resolution.

the two involved nuclei $\rho_1(\mathbf{r_1})$ and $\rho_2(\mathbf{r_2})$:

$$V(r) = \int d\mathbf{r}_1 d\mathbf{r}_2 \rho_1(\mathbf{r}_1)\rho_2(\mathbf{r}_2)V_{NN}(\mathbf{r}_1, \mathbf{r}_2, E), \qquad (2)$$

where r is the projectile-target distance and E is the energy per nucleon in the center-of-mass reference frame. The DFOL is a double folding potential obtained by a Love-Franey-type T-matrix interaction, but extended to lower energies, as discussed in detail in [45]. In the case of the SPP, a finite-range folding-type effective nucleon-nucleon interaction, in the context of the nonlocal model, is adopted. This interaction is quite similar to the M3Y interaction [46,47] in the surface region.

The densities $\rho_j(\mathbf{r_j})$ of projectile and target adopted in the foldings of both SPP and DFOL are parametrized by two-parameter Fermi-Dirac matter distributions profiles and are assumed to be spherical. The adopted density parameters (radius r and diffuseness a), listed in Table I for the different analysed potentials, are taken from Refs. [44] and [43], respectively. In particular, from the study of quasielastic barrier distribution of reactions induced by ^{18}O on medium-mass targets with SPP, the authors in Refs. [28,29,48–56] concluded that an effective way to correctly describe the data is to increase the diffuseness of the density matter profiles of ^{18}O from the SPP standard value ($a = 0.56$ fm) to 0.60–0.62 fm.

The imaginary part of the SPP was obtained from the real one by scaling its strength by a factor $N_W = 0.78$. This choice is the standard prescription for the SPP when calculations are performed in the DWBA [57] as was confirmed by a large number of cases [49–56]. For the DFOL potential, N_W was chosen in order to obtain a ratio of 0.78 between the volume integrals per nucleon of the imaginary and the real parts [J_W/J_V, see Eq. (3)], to follow the same criterion applied also for SPP. The SPP includes a local-equivalent contribution, that is an energy dependence given by a strength coefficient that accounts for Pauli nonlocality. Both potentials assume the same nuclear densities in the folding of the real and imaginary parts. This choice, although not justified by any strong theoretical reason, is done in order to minimize the number of parameters and it was found to be successful in the description of a large set of heavy-ion elastic scattering data [8,12,18,49–56].

TABLE I. Density parameters for the projectile and target of the ^{18}O + ^{76}Se collision adopted for the double folding potentials.

Potential	^{18}O projectile		^{76}Se target	
	r [fm]	a [fm]	r [fm]	a [fm]
DFOL	2.74	0.48	4.73	0.48
SPP	2.59	0.61	4.71	0.56

TABLE II. Mean radii $\langle R \rangle$ and volume integral per nucleon J for the real (V) and the imaginary (W) parts of the DFOL, SPP, and WS-fit potentials. Coefficient N_W of the imaginary part of the potential and total reaction cross section σ_R in the case of the DWBA and the CC calculations for the different potentials.

					DWBA		CC	
Potential	$\langle R_V \rangle$ [fm]	$\langle R_W \rangle$ [fm]	J_V [MeV fm^3]	J_W [MeV fm^3]	N_W	σ_R [mb]	N_W	σ_R [mb]
DFOL	4.91	4.79	-437	-341	0.84	2801	0.65	2753
SPP	5.02	5.02	-343	-268	0.78	2919	0.60	2836
WS-fit	8.84	8.98	-19	-22		3327		

A list of physical quantities associated to the calculations is given in Table II. In particular, the volume integral per nucleon was calculated by the following formula:

$$J_i = \frac{\int_0^{+\infty} 4\pi r^2 V_i(r) dr}{A_p A_t}, \tag{3}$$

in which A_p and A_t are the mass numbers of the projectile and the target, respectively, and $i = V$ or W for the real or imaginary potential, respectively.

The volume integrals of SPP and DFOL potentials, listed in Table II, are close to the typical values [6]. The total reaction cross sections for the two OPs, σ_R are listed in the same table, together with the average radii calculated using the formula

$$\langle R_i \rangle = \frac{\int 4\pi r^3 V_i(r) dr}{\int 4\pi r^2 V_i(r) dr}. \tag{4}$$

The comparison between the elastic experimental angular distribution and the OM calculations, performed with the two OPs, are shown in Fig. 3. The angular distribution is represented also in terms of transferred momentum:

$$q = \frac{2\sqrt{2\mu c^2 E_{\text{c.m.}}}}{\hbar c} \sin(\theta_{\text{c.m.}}/2), \tag{5}$$

where μ is the reduced mass of the system. Both calculations give a good description of the data for the angles smaller than the grazing one. At larger transferred momenta the other reaction channels start to compete with elastic scattering, making channel couplings more relevant and getting worse the accuracy of OM analysis. The description with the SPP is closer to the data than the one with DFOL. A possible reason is that, as already mentioned, the behavior of the ^{18}O was studied in details with the SPP. Other small differences can arise from the different systematics of mass-density used.

A fit with Woods-Saxon OP (WS-fit) has been performed using the SFRESCO routine to describe the shape of the experimental data. The depth, radius, and diffuseness of both real and imaginary parts were chosen in order to minimize the χ^2 of the resulting calculation, that is shown in Fig. 3. The values of the parameters emerging from the fit procedure are -11.187 MeV and -12.484 MeV for the depth, 0.74 fm and 0.93 fm for the diffuseness of the real and the imaginary part, respectively. The radii, the volume integral per nucleon, and the total reaction cross section are listed in Table II. Even if the description of the experimental data using this potential is very good, the obtained radii and the volume integrals per nucleon are far from the typical ones such as those obtained from SPP and DFOL OP (see Table II). Another fit was done by fixing the values of the diffuseness to a standard value (0.644 fm) leaving the other parameters free, but also in this case the radii and the volume integrals per nucleon are not reliable.

B. Couplings to the inelastic scattering channels

The contribution to the elastic cross section from couplings with inelastic and reaction channels is more important at large transferred momenta. The DWBA formalism is not appropriated to treat such kind of effects and a CC approach becomes necessary.

To perform CC calculations for the $^{18}\text{O} + ^{76}\text{Se}$ elastic and inelastic scattering, a crucial point is the choice of a proper coupling scheme. In this case, the CC calculations were performed using the explicit coupling of the elastic channel with some collective low-lying excited states of both projectile and target. The couplings to the inelastic channels were introduced through the use of a deformed complex coupling potential [42]. Indeed, in Ref. [12] it was proven that, in similar transferred momenta conditions, the coupled channel calculations are compatible with the experimental data if the low-lying excited states of both target and projectile are explicitly included in the coupling scheme. Moreover, only when the deformations of the imaginary part of the nuclear OP are properly included in the coupling potentials, the description of the experimental data becomes satisfactory. This evidence is in agreement with the Bohr-Mottelson unified model [58,59]. The coupling scheme adopted for the CC performed calculations includes the first 2^+ excited states of projectile and target at 1.982 MeV and 0.559 MeV, respectively, and the first 3^- state of the ^{18}O at 5.097 MeV.

The calculations for the inelastic channels were performed in DWBA and CC approaches in the context of a rotational model. Coulomb deformations of nuclei were introduced in terms of reduced transition probabilities. $B(E2; 0^+ \rightarrow 2^+) = 0.0043\, e^2\text{b}^2$, $B(E2; 0^+ \rightarrow 2^+) = 0.432\, e^2\text{b}^2$ were taken from Refs. [60,61] and used to describe Coulomb deformations of ^{18}O and ^{76}Se, respectively. The $B(E3) = 0.00125(5)\ e^2\text{b}^3$ for the ^{18}O was taken from Ref. [62]. The nuclear coupling potentials $V_\lambda^i(r)$ for $\lambda = 2, 3$ were treated in terms of their approximated expression, also described in Ref. [6], that is summarized in the following formula:

$$V_\lambda^i(r) = -\frac{\delta_\lambda^i}{\sqrt{4\pi}} \frac{dU_{\text{opt}}(r)}{dr}, \tag{6}$$

where δ_λ^i represents the deformation length and the index i refers to the projectile or target.

The deformation length is defined as [6]

$$\delta_\lambda^i = \beta_\lambda^i R_V = \frac{4\pi}{3Ze} \frac{\sqrt{(2I+1)B(E\lambda; I \to I')}}{R_V^{\lambda-1}}, \qquad (7)$$

where β_λ^i is the deformation parameter characterizing the transition (of multiple λ) of the given nucleus i of charge Ze and is deduced from the electric reduced transition probability $B(E\lambda; I \to I')$ from a state of spin I to a state of spin I'. The radii R_V of the two tested optical potentials are listed in Table II.

The inclusion of the imaginary part of the deformation was showed in Refs. [12,63,64] as a crucial aspect to obtain a good description of the experimental data. For the imaginary coupling potentials, the same radial form factors are assumed taking the $\beta_2^{\text{real}} = \beta_2^{\text{imag}}$ convention. The N_W coefficients adopted in the CC calculations are listed in Table II. When the couplings are explicitly included in the CC calculations, N_W is reduced to 0.6 for SPP, according to Ref. [13], and thus the corresponding value for DFOL is 0.65.

The theoretical results are compared with the experimental angular distributions of differential cross section for the transitions to the first excited states of the projectile (2^+ at 1.982 MeV) and the target (2^+ at 0.559 MeV) and to the transition in which both the projectile and target nuclei are in their first excited state in Fig. 4. They are in good agreement with experimental data collected for the first low-lying excited states.

The similarity between the CC and DWBA calculations prove that the channel coupling does not influence much the inelastic scattering angular distributions. The main effect is an attenuation of the oscillatory pattern, consistent with the experimental behavior. The DWBA one-step approach is missing in the angular distribution for the $2^+ \oplus 2^+$ transition at 2.542 MeV since it is a second order process. However, the agreement with the CC results is not satisfactory for this transition. A possible reason is that in the 2.5 MeV excitation energy region there are many excited states of the ^{76}Se nucleus which are not experimentally resolved and the contributions of such states could not be completely neglected at small angles, where the agreement with the data seems to be worst. In Fig. 5 the CC theoretical results for the two OPs are compared with the experimental data. In the insets of Figs. 3 and 5 a zoomed view of the Coulomb nuclear interference region is shown in linear scale to better determine the sensitivity to the potential [65,66]. The small differences between OM and CC calculations in the Coulomb nuclear interference region are within the already discussed 10% sensitivity. The data beyond the grazing angle ($\approx 10^\circ$) show a steeper slope than the one obtained in the DWBA calculations shown in Fig. 3. The effects due to the couplings with the low-lying excited states start to be important in the description of the elastic scattering beyond 12°, at almost 2.5 fm^{-1}, where the cross sections for the elastic and inelastic scattering channels become comparable. The couplings with the excited states produce sizable effects in this region and allow a very good description of the data.

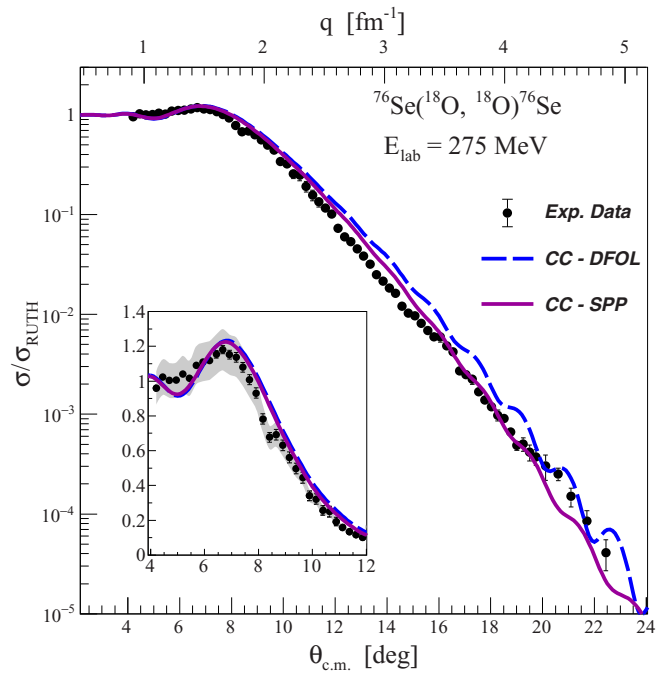

FIG. 5. Experimental elastic cross section angular distribution for the ^{18}O + ^{76}Se elastic scattering, compared to the results of CC calculations with the DFOL and SPP potentials. The theoretical curves are folded with the experimental angular resolution. Inset: zoomed view of the Coulomb nuclear interference region. The experimental data are shown together with a grey band corresponding to the 10% uncertainty due to the charge collection and target thickness (see text).

IV. CONCLUSIONS

Elastic and inelastic scatterings for the ^{18}O + ^{76}Se collision at 275 MeV incident energy were studied for the first time. Thanks to the large acceptance of the MAGNEX spectrometer, a wide range of transferred momenta was explored in only three angular settings. The overlap between the measured cross sections for the different spectrometer angular settings shows a good agreement between independent measurements. The ground-to-ground state transition was isolated from the first 2^+ excited state thanks to the good energy resolution obtained by a careful tuning of the experimental setup and thanks to the advanced techniques applied during the data reduction. A broad range of cross sections was explored, covering, for the elastic scattering, eight orders of magnitude always keeping an high significance level.

The experimental results were compared with cross section calculations performed with FRESCO. Some of the most advanced OPs, in particular DFOL and SPP, were scrutinized to study their capability to describe the measured elastic scattering cross sections. The description of the data is not fully satisfactory beyond the grazing angle if such calculations are performed in the OM formalism.

A good description of the data in OM was obtained considering a Woods-Saxon potential whose parameters are fitted on the experimental data. However, this technique generates an OP whose integral properties deviate much from systematics. Moreover, it would not be predictive for other systems where

the elastic channel is not experimentally measurable, e.g., for the reaction channels of interest for the NUMEN project [4].

It was found that at large transferred momenta the effect of couplings with first low-lying excited states is crucial to correctly describe the angular distribution of differential cross sections. To determine the inelastic flux and its effect on the elastic channel, DWBA and CC calculations were performed. The first collective states of the colliding nuclei were included. Inclusion of only the first 2^+ of the projectile and target and the first 3^- of the ^{18}O collective low-lying excited states turned out to be enough to well describe almost all the angular distributions over the full range of transferred momenta explored.

This study suggests that the couplings to low-lying collective states in even-even nuclei are crucial degrees of freedom for an accurate extraction of nuclear structure information from NUMEN data.

ACKNOWLEDGMENTS

This project received funding from the European Research Council (ERC) under the Nov 14 European Union's Horizon 2020 research and innovation programme (NURE project, Grant Agreement No. 714625). Support from the Brazilian funding agencies FAPESP Proc. No. 2019/07767-1 and INCT-FNA Proc. No. 464898/2014-5 is acknowledged. The Mexican authors acknowledge partial financial support from CONACyT 314857 and DGAPA-PAPIIT IN107820 and IG101120.

[1] H. Lenske *et al.*, Prog. Part. Nucl. Phys. **109**, 103716 (2019).
[2] H. Ejiri, J. Suhonen, and K. Zuber, Phys. Rep. **797**, 1 (2019).
[3] M. Cavallaro *et al.*, in *55th International Winter Meeting on Nuclear Physics (BORMIO2017)*, Vol. 302 (POS, 2017).
[4] F. Cappuzzello *et al.*, Eur. Phys. J. A **54**, 72 (2018).
[5] P. E. Hodgson, *Nuclear Reactions and Nuclear Structure* (Clarendon Press, Oxford, 1971).
[6] G. R. Satchler, *Direct Nuclear Reactions* (Oxford University Press, Oxford, 1983), p. 619.
[7] N. Glendenning, *Direct Nuclear Reactions* (Academic Press, Inc., New York, 1983).
[8] D. Carbone, J. L. Ferreira, S. Calabrese, F. Cappuzzello, M. Cavallaro, A. Hacisalihoglu, H. Lenske, J. Lubian, R. I. Magnaña Vsevolodovna, E. Santopinto, C. Agodi, L. Acosta, D. Bonanno, T. Borello-Lewin, I. Boztosun, G. A. Brischetto, S. Burrello, D. Calvo, E. R. ChavezLomeli, I. Ciraldo *et al.*, Phys. Rev. C **102**, 044606 (2020).
[9] D. Khoa, W. Von Ortezen, H. G. Bohelen, and S. Ohkubo, J. Phys. G **34**, 111 (2007).
[10] S. Ohkubo and Y. Hirabayashi, Phys. Rev. C **89**, 051601(R) (2014).
[11] S. Ohkubo and K. Yamashita, Phys. Rev. C **66**, 021301(R) (2002).
[12] V. A. B. Zagatto, F. Cappuzzello, J. Lubian, M. Cavallaro, R. Linares, D. Carbone, C. Agodi, A. Foti, S. Tudisco, J. S. Wang, J. R. B. Oliveira, and M. S. Hussein, Phys. Rev. C **97**, 054608 (2018).
[13] D. Pereira, J. Lubian, J. R. B. Oliveira, D. P. de Sousa, and L. C. Chamon, Phys. Lett. B **670**, 330 (2009).
[14] D. Pereira *et al.*, Phys. Lett. B **710**, 426 (2012).
[15] J. R. B. Oliveira *et al.*, J. Phys. G. Nucl. Part. Phys. **40**, 105101 (2013).
[16] F. Cappuzzello, D. Nicolosi, R. Linares, J. R. B. Oliveira, J. Lubian, C. Agodi, D. Carbone, M. Cavallaro, P. N. de Faria, A. Foti, and M. R. D. Rodrigues, Eur. Phys. J. A **52**, 169 (2016).
[17] F. Cappuzzello *et al.*, Nucl. Instrum. Methods Phys. Res. A **763**, 314 (2014).
[18] A. Spatafora, F. Cappuzzello, D. Carbone, M. Cavallaro, J. A. Lay, L. Acosta, C. Agodi, D. Bonanno, D. Bongiovanni, I. Boztosun, G. A. Brischetto, S. Burrello, S. Calabrese, D. Calvo, E. R. ChavezLomeli, I. Ciraldo, M. Colonna, F. Delaunay, N. Deshmukh, J. L. Ferreira *et al.*, Phys Rev. C **100**, 034620 (2019).
[19] K. E. Rehm *et al.*, Phys Rev. C **12**, 1945 (1975).
[20] H. G. Bohlen *et al.*, Z. Phys. **273**, 211 (1975).
[21] W. G. Love, T. Terasawa, and G. R. Satchler, Nucl. Phys. A **291**, 183 (1977).
[22] S. Salem-Vasconcelos, E. M. Takagui, M. J. Bechara, K. Koide, O. Dietzsch, A. B. Nuevo, Jr., and H. Takai, Phys. Rev. C **50**, 927 (1994).
[23] P. K. Sahu, R. K. Choudhury, D. C. Biswas, and B. K. Nayak, Phys. Rev. C **64**, 014609 (2001).
[24] J. Lachkar *et al.*, Phys. Rev. C **14**, 933 (1976).
[25] R. Lecomte *et al.*, Nucl. Phys. A **284**, 123 (1977).
[26] H. R. Burgl *et al.*, Nucl. Phys. A **334**, 413 (1980).
[27] J. D. Zumbro *et al.*, Nucl. Phys. A **393**, 15 (1983).
[28] E. Crema, D. R. Otomar, R. F. Simoes, A. Barioni, D. S. Monteiro, L. K. Ono, J. M. B. Shorto, J. Lubian, and P. R. S. Gomes, Phys. Rev. C **84**, 024601 (2011).
[29] E. Crema, V. A. B. Zagatto, J. M. B. Shorto, B. Paes, J. Lubian, R. F. Simoes, D. S. Monteiro, J. F. P. Huiza, N. Added, M. C. Morais, and P. R. S. Gomes, Phys. Rev. C **98**, 044614 (2018).
[30] L. Rifuggiato, D Calabretta and G. Cuttone, in *Ciclotrons and Their Applications: Proceedings of the 17th International Conference*, Cyclotrons 2004, edited by A. Goto (Particle Accelerator Society of Japan, Tokyo, 2004).
[31] F. Cappuzzello, C. Agodi, D. Carbone and M. Cavallaro, Eur. Phys. J. A **52**, 167 (2016).
[32] D. Torresi *et al.*, Nucl. Instrum. Methods Phys. Res. A **989**, 164918 (2021).
[33] M. Cavallaro, F. Cappuzzello, D. Carbone, R. Linares, D. Torresi, L. Acosta, C. Agodi, D. Bonanno, D. Bongiovanni *et al.*, Nucl. Instrum. Methods Phys. Res. A **637**, 77 (2011).
[34] D. Carbone, Eur. Phys. J. Plus **130**, 143 (2015).
[35] F. Cappuzzello, M. Cavallaro, A. Cunsolo, A. Foti, D. Carbone, S. E. A. Orrigo, and M. R. D. Rodrigues, Nucl. Instrum. Methods Phys. Res. A **621**, 419 (2010).
[36] S. Calabrese, F. Cappuzzello, D. Carbone, M. Cavallaro, C. Agodi, L. Acosta, D. Bonanno, D. Bongiovanni, T. Borello-Lewin, I. Boztosun *et al.*, Acta Phys. Polon. B **49**, 275 (2018).
[37] M. Cavallaro, C. Agodi, G. A. Brischetto, S. Calabrese, F. Cappuzzello, D. Carbone, I. Ciraldo, A. Pakou, O. Sgouros, V.

Soukeras *et al.*, Nucl. Instrum. Methods Phys. Res. B **463**, 334 (2020).
[38] S. Calabrese, F. Cappuzzello, D. Carbone, M. Cavallaro *et al.*, Nucl. Instrum. Methods Phys. Res. A **980**, 164500 (2020).
[39] F. Cappuzzello, D. Carbone, and M. Cavallaro, Nucl. Instrum. Methods Phys. Res. A **638**, 74 (2011).
[40] A. Cunsolo, F. Cappuzzello, A. Foti, A. Lazzaro, A. L. Melita, C. Nociforo, V. Shchepunov, and J. S. Winfield, Nucl. Instrum. Methods Phys. Res. A **484**, 56 (2002).
[41] B. Singh, Nucl. Data Sheets **74**, 63 (1995)
[42] I. J. Thompson, Comput. Phys. Rep. **7**, 167 (1988).
[43] H. Lenske, private communication.
[44] L. C. Chamon, B. V. Carlson, L. R. Gasques, D. Pereira, C. De Conti, M. A. G. Alvarez, M. S. Hussein, M. A. Candido Ribeiro, E. S. Rossi, Jr., and C. P. Silva, Phys. Rev. C **66**, 014610 (2002).
[45] H. Lenske, J. I. Bellone, M. Colonna, and J.-A. Lay, Phys. Rev. C **98**, 044620 (2018).
[46] G. R. Satchler and W. G. Love, Phys. Rep. **55**, 183 (1979).
[47] M. E. Brandan and G. R. Satchler, Phys. Rep. **285**, 143 (1997), and references therein.
[48] L. M. Fonseca, R. Linares, V. A. B. Zagatto, F. Cappuzzello, D. Carbone, M. Cavallaro, C Agodi, J. Lubian, and J. R. B. Oliveira, Phys. Rev. C **100**, 014604 (2019).
[49] B. Paes, G. Santagati, R. M. Vsevolodovna, F. Cappuzzello, D. Carbone, E. N. Cardozo, M. Cavallaro, H. Garcia-Tecocoatzi, A. Gargano, J. L. Ferreira, S. M. Lenzi, R. Linares, E. Santopinto, A. Vitturi, and J. Lubian, Phys. Rev. C **96**, 044612 (2017).
[50] D. Carbone, J. L. Ferreira, F. Cappuzzello, J. Lubian, C. Agodi, M. Cavallaro, A. Foti, A. Gargano, S. M. Lenzi, R. Linares, and G. Santagati, Phys. Rev C **95**, 034603 (2017).
[51] E. N. Cardozo, J. Lubian, R. Linares, F. Cappuzzello, D. Carbone, M. Cavallaro, J. L. Ferreira, A. Gargano, B. Paes, and G. Santagati, Phys. Rev. C **97**, 064611 (2018).
[52] R. Linares, M. J. Ermamatov, J. Lubian, F. Cappuzzello, D. Carbone, E. N. Cardozo, M. Cavallaro, J. L. Ferreira, A. Foti, A. Gargano, B. Paes, G. Santagati, and V. A. B. Zagatto, Phys. Rev. C **98**, 054615 (2018).
[53] M. J. Ermamatov, R. Linares, J. Lubian, J. L. Ferreira, F. Cappuzzello, D. Carbone, M. Cavallaro, M. Cubero, P. N. de Faria, A. Foti, G. Santagati, and V. A. B. Zagatto, Phys. Rev C **96**, 044603 (2017).
[54] D. Carbone, R. Linares, P. Amador-Valenzuela, S. Calabrese, F. Cappuzzello, M. Cavallaro, S. Firat, M. Fisichella, A. Spatafora, and L. Acosta, Universe **7**, 58 (2021).
[55] M. Cavallaro, J. I. Bellone, S. Calabrese, C. Agodi, S. Burrello, F. Cappuzzello, D. Carbone, M. Colonna, N. Deshmukh, and H. Lenske, Front. Astron. Space Sci. **8**, 659815 (2021).
[56] J. L. Ferreira, D. Carbone, M. Cavallaro, N. N. Deshmukh, C. Agodi, G. A. Brischetto, S. Calabrese, F. Cappuzzello, E. N. Cardozo, I. Ciraldo, M. Cutuli, M. Fisichella, A. Foti, L. La Fauci, O. Sgouros, V. Soukeras, A. Spatafora, D. Torresi, and J. Lubian, Phys. Rev. C **103**, 054604 (2021).
[57] M. A. G. Alvarez *et al.*, Nucl. Phys. A **723**, 93 (2003).
[58] K. Alder *et al.*, Rev. Mod. Phys. **28**, 432 (1956).
[59] D. L. Hill and J. A. Wheeler, Phys. Rev. **89**, 1102 (1953).
[60] P. Moller, A. J. Sierk, T. Ichikawa, and H. Sagawa, At. Data Nucl. Data Tables **109**, 1 (2016).
[61] B. Pritychenko, M. Birch, B. Singh, and M. Horoi, At. Data Nucl. Data Tables **107**, 1 (2016).
[62] T. Kibedi, At. Data Nucl. Data Tables **80**, 35 (2002).
[63] G. R. Satchler, Phys. Lett. B **33**, 385 (1970).
[64] I. Boztosun, M. Karakoc, and Y. Kucuk, Phys. Rev. C **77**, 064608 (2008).
[65] G. R. Satchler, Nucl. Phys. A **579**, 241 (1994).
[66] J. B. Ball, C. B. Fulmer, E. E. Gross, M. L. Halbert, D. C. Hensley, C. A. Ludemann, M. J. Saltmarsh, and G. R. Satchler, Nucl. Phys. A **252**, 208 (1975).